PAPER • OPEN ACCESS

Joint EURADOS WG9-WG11 rem-counter intercomparison in a Mevion S250i proton therapy facility with Hyperscan pulsed synchrocyclotron

To cite this article: Gabriele Zorloni *et al* 2022 *Phys. Med. Biol.* **67** 075005

IOP Publishing Phys. Med. Biol. 67 (2022) 075005 https://doi.org/10.1088/1361-6560/ac5b9c

Physics in Medicine & Biology

IPEM Institute of Physics and Engineering in Medicine

PAPER

Joint EURADOS WG9-WG11 rem-counter intercomparison in a Mevion S250i proton therapy facility with Hyperscan pulsed synchrocyclotron

Gabriele Zorloni[1], Geert Bosmans[2], Thomas Brall[3], Marco Caresana[4], Marijke De Saint-Hubert[5], Carles Domingo[6], Christian Ferrante[4], Francesca Ferrulli[1,7], Renata Kopec[8], Johannes Leidner[1], Vladimir Mares[3], Racell Nabha[5], Pawel Olko[8], Miguel Angel Caballero-Pacheco[6], Werner Rühm[3], Marco Silari[1], Liliana Stolarczyk[8,9], Jan Swakon[8], Marco Tisi[3], Sebastian Trinkl[10], Olivier Van Hoey[5] and Gloria Vilches-Freixas[2]

[1] CERN, 1211 Geneva 23, Switzerland
[2] Department of Radiation Oncology (MAASTRO), GROW—School for Oncology, Maastricht University Medical Centre, Maastricht, The Netherlands
[3] Helmholtz Zentrum München, Institute of Radiation Medicine, Ingolstädter Landstr. D-1, 85764 Neuherberg, Germany
[4] Department of Energy, Polytechnic of Milan, via Lambruschini 4, I-20156, Milan, Italy
[5] Belgian Nuclear Research Center SCK CEN, B-2400 Mol, Belgium
[6] Universitat Autònoma de Barcelona, Departament de Física, E-08193 Bellaterra, Spain
[7] University of Caen Normandy, F-14032 Caen 5, France
[8] Institute of Nuclear Physics PAN, Radzikowskiego 152, 31-342 Krakow, Poland
[9] The Danish Centre for Particle Therapy, Aarhus University Hospital, Palle Juul-Jensens Boulevard 25, DK-8200 Aarhus, Denmark
[10] Federal Office for Radiation Protection, Medical and Occupational Radiation Protection, Ingolstädter Landstraße 1, D-85764 Neuherberg, Germany

E-mail: gabriele.zorloni@cern.ch

Keywords: pulsed field dosimetry, rem-counter, neutron dosimetry, dosimetry at accelerators

OPEN ACCESS

RECEIVED
10 November 2021

REVISED
24 February 2022

ACCEPTED FOR PUBLICATION
8 March 2022

PUBLISHED
28 March 2022

Abstract

Objective. Proton therapy is gaining popularity because of the improved dose delivery over conventional radiation therapy. The secondary dose to healthy tissues is dominated by secondary neutrons. Commercial rem-counters are valuable instruments for the on-line assessment of neutron ambient dose equivalent ($H^*(10)$). In general, however, *a priori* knowledge of the type of facility and of the radiation field is required for the proper choice of any survey meter. The novel Mevion S250i Hyperscan synchrocyclotron mounts the accelerator directly on the gantry. It provides a scanned 227 MeV proton beam, delivered in pulses with a pulse width of 10 μs at 750 Hz frequency, which is afterwards degraded in energy by a range shifter modulator system. This environment is particularly challenging for commercial rem-counters; therefore, we tested the reliability of some of the most widespread rem-counters to understand their limits in the Mevion S250i stray neutron field.
Approach. This work, promoted by the European Radiation Dosimetry Group (EURADOS), describes a rem-counter intercomparison at the Maastro Proton Therapy centre in the Netherlands, which houses the novel Mevion S250i Hyperscan system. Several rem-counters were employed in the intercomparison (LUPIN, LINUS, WENDI-II, LB6411, NM2B-458, NM2B-495Pb), which included simulation of a patient treatment protocol employing a water tank phantom. The outcomes of the experiment were compared with models and data from the literature. *Main results*. We found that only the LUPIN allowed for a correct assessment of $H^*(10)$ within a 20% uncertainty. All other rem-counters underestimated the reference $H^*(10)$ by factors from 2 to more than 10, depending on the detector model and on the neutron dose per pulse. In pulsed fields, the neutron dose per pulse is a fundamental parameter, while the average neutron dose rate is a secondary quantity. An average 150–200 $\mu Sv/Gy_{RBE}$ neutron $H^*(10)$ at various positions around the phantom and at distances between 186 cm and 300 cm from it was measured per unit therapeutic dose delivered to the target.
Significance. Our results are partially in line with results obtained at similar Mevion facilities

employing passive energy modulation. Comparisons with facilities employing active energy modulation confirmed that the neutron $H^*(10)$ can increase up to more than a factor of 10 when passive energy modulation is employed. The challenging environment of the Mevion stray neutron field requires the use of specific rem-counters sensitive to high-energy neutrons (up to a few hundred MeV) and specifically designed to withstand pulsed neutron fields.

1. Introduction

Proton therapy is gaining popularity, in particular for the treatment of children and adolescents, because of the improved dose distribution, which implies reduced entrance dose, null exit dose and high ballistic precision (Park *et al* 2011, Linz 2012, De Saint-Hubert *et al* 2016, Howell *et al* 2016). The out-of-field dose, which might lead to the occurrence of secondary cancer, is dominated by stray neutrons (Hall 2006, Jarlskog and Paganetti 2008, Schneider and Hälg 2015, Hälg and Schneider 2020). Internal neutrons are directly produced within the patient, whilst external neutrons are produced within the beam delivery system and the walls of the treatment room. While the production of internal neutrons depends on the treatment plan, the production of external neutrons is facility dependent. The latter component is enhanced in accelerators using an absorber to degrade the proton energy (Gottschalk 2006, Paganetti *et al* 2006, Carnicer *et al* 2013). In any case, precise and accurate neutron monitoring systems are crucial during the commissioning and the operational phases of proton therapy facilities.

Neutron energy spectra produced in proton therapy range from thermal energies up to the maximum energy of the proton beam. The neutron fluence to ambient dose equivalent conversion coefficients from ICRP-74/ICRU-57 ($h^*(10)$) strongly depend on the neutron energy, reaching their maximum around a few tens of MeV (ICRP-74 1996, ICRU-57 1998).

Rem-counters are widely used instruments for directly assessing the neutron ambient dose equivalent ($H^*(10)$) (Knoll 2010). Their response function satisfactorily approximates the $h^*(10)$ coefficients over a wide energy range. Conventional rem-counters can accurately measure $H^*(10)$ up to energies of about 15 MeV. Extended-range rem-counters, i.e. rem-counters which mount high-Z inserts which promote (n,xn) reactions (Birattari *et al* 1990), are capable of measuring $H^*(10)$ up to energies of several hundred MeV and should therefore be preferred at proton therapy facilities.

Depending on the model, commercial rem-counters are characterized by a shaping time of the output voltage signal in the range 1–3 μs that, for a semi-Gaussian shaping, results in a dead time in the range 5–15 μs. This corresponds to the minimum time interval that must separate two events in order that they can be recognized as two separate/independent signals (Knoll 2010). The dead time therefore determines the maximum dose rate measurable by a rem-counter without incurring in severe count losses.

The time structure of the stray neutron field in proton therapy facilities is the same of the proton beam. For pulsed beams with pulse width of the order of 10–20 μs or less, the key parameter determining the rem-counter response is the neutron Dose Per Pulse (DPP), rather than the dose rate averaged over seconds: neutrons reach the detector within a time width shorter than the dead time, and in principle only a single count can be collected per each pulse (Justus 2012). In reality, the neutron thermalization and drift process in the rem-counter moderator, which takes 300–700 μs on average, partially mitigates the problem (Caresana *et al* 2014). Consequently, the higher the DPP, the higher the probability of losing counts within a single pulse (Leake *et al* 2010, Justus 2012). Caresana *et al* reported an extended study of this effect for several commercial rem-counters (Caresana *et al* 2014): for the majority of the tested instruments, linearity started failing at around 10 nSv/pulse, although in a very few cases it stretched up to 500 nSv/pulse.

Working Groups (WGs) 9 and 11 of the European Radiation Dosimetry Group (EURADOS) recently organized three joint intercomparison experiments at the Maastro Proton Therapy centre (Maastricht, the Netherlands). The facility houses a Mevion (Mevion Medical Systems, 300 Foster St. Littleton, MA 01460, US) S250i Hyperscan synchrocyclotron (Vilches-Freixas *et al* 2020), which distinguishes from all other commercial proton therapy units by the pulsed structure of the beam. The machine delivers 227 MeV protons with a pulsed time profile (10 μs pulse width, up to 8 pC/pulse), which are then degraded in energy to yield the required clinical volume. The resulting radiation environment is then particularly challenging for reliably assessing $H^*(10)$ from secondary neutrons with commercial rem-counters. In fact, the pulsed structure of the beam, which generally requires caution in the use of active rem-counters (Justus 2012, Caresana *et al* 2014), is combined with passive energy degradation of the primary beam, which results in an enhanced neutron production, and so DPP, with respect to active systems (Paganetti *et al* 2006).

The three EURADOS experiments aimed at investigating the secondary neutron dose employing different techniques. The first experiment focused on in-phantom neutron dosimetry using passive dosimeters. The

Table 1. Rem-counters used in the experiment.

Instrument	Calibration factor (nSv per count)	Calibration spectrum	Extended range	Institute
LUPIN	0.47	Pu-Be	Yes	Politecnico di Milano (PoliMi)
LINUS	0.89	Am-Be	Yes	CERN
Wendi-II	0.31[a]	Cf-252	Yes	SCK CEN
Wendi-II	0.31[a]	Pu-Be	Yes	IFJ
NM2B-458	0.97	Am-Be	No	HMGU
NM2B-495Pb[b]	0.93	Am-Be	Yes	HMGU
LB6411	0.35[a]	Cf-252	No	SCK CEN
LB6411	0.35	Am-Be	No	Universitat Autònoma de Barcelona (UAB)
LB6411	0.35[a]	Am-Be	No	Skandion kliniken

[a] Data taken from the rem-counter datasheet.

[b] The device was characterized with quasi-monoenergetic neutrons (up to 400 MeV) at the Research Centre for Nuclear Physics (RCNP) in Osaka, Japan (Mares *et al* 2017).

second experiment focused on ambient neutron spectrometry, by comparing Monte Carlo calculations with Bonner sphere measurements.

This paper focuses on the third experiment, which was designed to test rem-counters in the Mevion stray field, with emphasis on its pulsed time structure. We compared nine commercial rem-counters placed at nine different positions around the treatment isocentre while irradiating a water tank phantom simulating a patient treatment protocol. The goals of this intercomparison were:

1. To compare the performance of some of the most used commercial rem-counters in a pulsed proton therapy facility with passive energy degradation at clinical beam settings.
2. To compare our results with literature models, and, in particular, to verify whether the rem-counter underestimations here observed were in line with theoretical expectations.
3. To compare the measured neutron $H^*(10)$ with values measured in previous experiments performed at other clinical facilities, in particular with respect to non-pulsed proton beams delivered with active energy selection.

2. Materials and methods

2.1. Description of the facility

The Mevion S250i Hyperscan system is a compact 10 T field synchrocyclotron which requires a single vault of limited dimensions. The Maastro Proton Therapy centre is the first European facility housing this type of accelerator, which is directly mounted on a rotating system (gantry) that also incorporates the beam monitors, range modulator and multi-leaf collimator (Vilches-Freixas *et al* 2020). The proton spots are delivered along the transverse plane through a pair of scanning magnets. The depth of the Bragg peak is modulated by an energy degrader consisting of 18 Lexan (polycarbonate) plates that can be placed in the path of the proton beam according to the required energy. The minimum proton energy available is 13.49 MeV for superficial tumours, the maximum 227 MeV corresponding to a depth in water of 32.2 cm. At the end of the beam line, the nickel-alloy multi-leaf collimator conforms (trims) the beam to reduce the lateral penumbra.

The beam is delivered with a maximum frequency of roughly 750 Hz, which corresponds to a minimum time between pulses of roughly 1.3 ms. Since the time structure of the neutron field reflects that of the proton beam, it can be considered as a pulsed neutron field. Each neutron pulse is recognized by the rem-counters as a single isolated event, i.e. with a minimum time between pulses of 1.3 ms that is much longer than the 5–15 μs dead time typical for commercial rem-counters.

2.2. Description of the rem-counters

Table 1 lists the rem-counters and their respective calibration factors. A more detailed description is given below.

2.2.1. LUPIN

The LUPIN (Long interval, Ultra-wide dynamic range, pile-up free, Neutron rem-counter) from ELSE Nuclear (ELSE Nuclear, via Riccardo Pitteri 10, Milan, Italy) is an extended-range rem-counter, using a BF_3 proportional

counter, specifically designed for monitoring pulsed neutron fields (Caresana *et al* 2013a, 2013b, Ferrarini *et al* 2010). The BF_3 counter is placed in a cylindrical polyethylene moderator with lead and cadmium inserts. The front-end electronics is based on a logarithmic amplifier. The LUPIN used during the intercomparison allowed the real-time reading of $H^*(10)$ with an integration time of 1 s. Therefore, it was possible to reconstruct and analyse $H^*(10)$ variations with 1 s time resolution. The detection capabilities of the LUPIN were demonstrated both in terms of response to high-energy neutrons (Caresana *et al* 2014b, Dinar *et al* 2018) and in pulsed fields (Aza *et al* 2014, Caresana *et al* 2014). The LUPIN was chosen as the reference rem-counter in this intercomparison. This choice proved to be adequate, as discussed in section 3.

2.2.2. LINUS

The LINUS (Long Interval NeUtron Survey meter) is the original extended-range rem-counter developed about 30 years ago from an Andersson-Braun device (Birattari *et al* 1990, 1992, 1993, 1998). The instrument comprises a ^{3}He proportional counter placed within a spherical polyethylene moderator. The moderator incorporates a boron-doped synthetic rubber absorber and a 1 cm thick lead shell. Its response function extends up to more than 400 MeV.

2.2.3. WENDI-II

The WENDI-II (Wide Energy Neutron Detection Instrument) from Thermo Scientific (Thermo Fisher Scientific, 168 Third Avenue, Waltham, Massachusetts, US) is an extended-range rem-counter designed to measure $H^*(10)$ up to 5 GeV (Olsher *et al* 2000). It includes a ^{3}He proportional counter surrounded by a cylindrical polyethylene moderator and a layer of tungsten powder.

2.2.4. Berthold LB6411

The Berthold LB6411 (Berthold Technologies GmbH & Co.KG, Calmbacher Str. 22, Bad Wildbad, Germany) is a rem-counter designed to measure $H^*(10)$ up to 20 MeV with a measuring range from a few tens of nSv h^{-1} to 100 mSv h^{-1} (Burgkhardt *et al* 1997). It includes a cylindrical ^{3}He/methane proportional counter surrounded by a spherical polyethylene moderator and perforated cadmium absorbers.

2.2.5. NM2B-458 and NM2B-495Pb

Two NM2B rem-counters (Nuclear Enterprises Technology Ltd., Benham, Berkshire, UK) were tested. The conventional NM2B-458 includes a BF_3 proportional counter surrounded by an inner polyethylene moderator, a boron-doped synthetic rubber absorber, and an outer polyethylene moderator. The extended-range NM2B-495Pb includes a lead shell surrounding the boron-doped rubber. The response functions of both rem-counters were calculated by means of Monte Carlo simulations (Mares *et al* 2002).

2.3. Experimental setup

A water tank phantom (30 cm × 30 cm × 60 cm) was employed to simulate a patient treatment protocol. A single beam plan was made in Raystation v.9A using inverse planning with a prescribed dose of 10 Gy_{RBE}[11] to a 15 cm × 15 cm × 15 cm cube centred at 15 cm depth in water. The multi-leaf collimator was used to laterally trim the field, reducing the penumbra. The energies ranged from 175.9 MeV to 115.8 MeV for a total of 14 energy layers. The spot spacing ranged from 0.5 cm to 0.6 cm. These beam settings were considered representative of a clinical beam, and therefore they allowed evaluating the reliability of commercial rem-counters in treatment-like conditions.

The nine rem-counters were aligned to the isocentre height (125 cm above the floor), and measured $H^*(10)$ at nine positions around the water tank, as shown in figure 1. After each session, all rem-counters changed position, so that each detector measured $H^*(10)$ at each position under the same experimental conditions.

2.4. Mathematical model for the data analysis

After preliminary data analysis (section 3.1), all rem-counters appeared to strongly underestimate $H^*(10)$ with respect to the LUPIN. To check the consistency of these results with literature data, an empirical model taken from Caresana *et al* (2014) was used. The model assumes that, given the reference (conventionally true) DPP, D_{ref}, the expected DPP provided by a certain rem-counter, D_{meas}, can be calculated as:

$$D_{meas} = \frac{D_{ref}}{1 + (D_{ref}/D_{half})}, \quad (1)$$

[11] In proton therapy, the relative biological effectiveness (RBE) to convert from the physical absorbed dose, expressed in Gy, to the therapeutic dose, expressed in Gy_{RBE}, is 1.1 (1 Gy = 1.1 Gy_{RBE}) (Paganetti et al 2002).

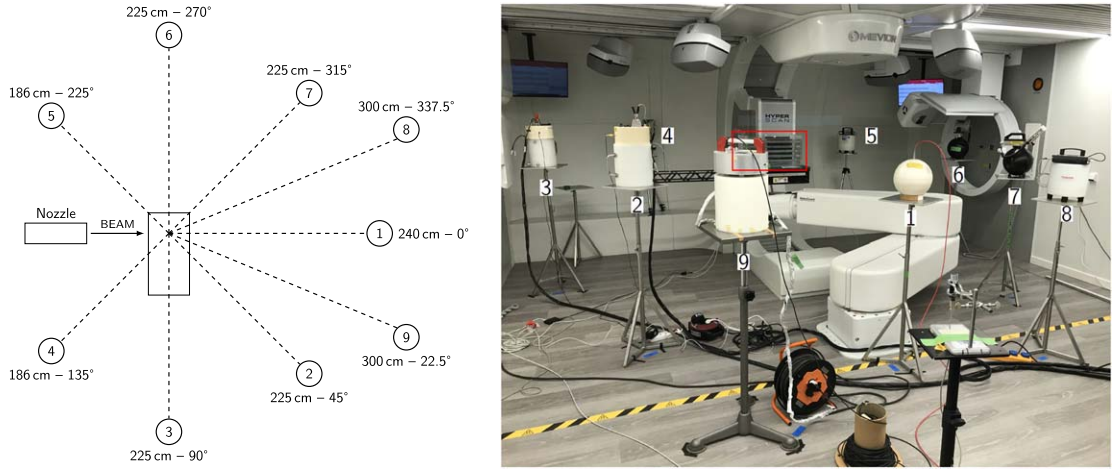

Figure 1. Schematic of the measurement positions around the water tank (left) and a picture of the measurement setup (right). In the schematic, at each measurement position, the numbers represent the distance to isocentre in centimetres and the angle with respect to the beam direction. In the picture, the water tank phantom is in the background identified by the red rectangle, partially hidden by the LUPIN in position 9.

where the coefficient D_{half}, with the same dimensions as the DPP (nSv/pulse), corresponds to the DPP for which $D_{meas} = D_{ref}/2$. D_{half} depends on the type of rem-counter only, and its value is tabulated for many commercial rem-counters in Caresana *et al* (2014).

D_{ref} can be estimated by correcting the output of the reference instrument by its own D_{half}:

$$D_{ref} = \frac{D_{meas}}{1 - (D_{meas}/D_{half})}. \tag{2}$$

It follows that the reference instrument should possess a $D_{half} \gg D_{meas}$.

Commercial rem-counters are not able to instantaneously provide D_{meas}, because they integrate the total dose over a certain period of time longer than their dead time. In our experiment, all rem-counters were read after the end of each irradiation. The only exception was the LUPIN, which allowed the real time reading of $H^*(10)$ with 1 s time resolution. By combining the $H^*(10)$ trend from the LUPIN with the information displayed per each single pulse in the accelerator log files (in particular the delivery time, see section 3.1 for details), for each second an equivalent series of D_{meas} for the LUPIN (hereafter D_{LUPIN}) and D_{ref} values were obtained from equation (2).

Therefore, it was possible to predict the theoretical D_{meas} of each other rem-counter from equation (1), hereafter called D_{model}: per each pulse i, the DPP $D_{model,i,k,j}$ was calculated for each rem-counter j at position k. Assuming valid the model, $D_{model,i,k,j}$ is the expected DPP indicated by a specific rem-counter j. $D_{model,i,k,j}$ is normalized to $D_{LUPIN,i,k}$ and summed over the duration of the irradiation as in equation (3):

$$U_{model,k,j} = \frac{\sum_i^N D_{model,i,k,j}}{\sum_i^N D_{LUPIN,i,k}}. \tag{3}$$

$U_{model,k,j}$ is the expected underestimation foreseen by the model for the jth rem-counter in the kth position. The value at the denominator of equation (3) is by definition equal to the experimental $H^*(10)$ measured by the LUPIN at the end of the irradiation, but for the sake of clarity the denominator is constructed using the same expression as the numerator.

$U_{model,k,j}$ can then be compared with the measured underestimation (U_{exp}), which was the datum available at the end of each irradiation.

3. Results and discussion

3.1. Results

Table 2 lists the $H^*(10)$ values in $\mu Sv/Gy_{RBE}$ measured by each rem-counter at each position (normalized to unit therapeutic dose at the isocentre). The total delivered therapeutic dose to the water phantom was chosen to guarantee a measurement uncertainty due to Poisson counting statistics well below 10% (total neutron $H^*(10)$ per session up to a few mSv). However, considering the uncertainties related to (1) calibration, (2) position and (3) angular/energy response functions of the rem-counters, the final overall uncertainty can be assumed to be

Table 2. $H^*(10)$ ($\mu Sv/Gy_{RBE}$) measured by the nine rem-counters at the nine positions around the water phantom, normalised to 1 Gy_{RBE} at the isocentre. The uncertainties are expressed as one standard deviation around the measured value ($k = 1$).

	$H^*(10)$ ($\mu Sv/Gy_{RBE}$)								
Position	LUPIN (PoliMi)	LINUS (CERN)	WENDI-II (SCK CEN)	WENDI-II (IFJ)	NM2B-458 (HMGU)	NM2B-495Pb (HMGU)	LB6411 (SCK CEN)	LB6411 (Skandion)	LB6411 (UAB)
1	133.2 ± 26.5	16.0 ± 3.2	43.4 ± 8.7	39.7 ± 8.0	—	18.9 ± 3.8	21.1 ± 8.4	22.2 ± 8.9	—
2	99.2 ± 19.8	16.8 ± 3.4	36.2 ± 7.26	35.4 ± 7.1	9.6 ± 3.8	14.7 ± 3.0	—	21.9 ± 8.8	21.4 ± 8.6
3	97.8 ± 19.5	17.9 ± 3.6	36.9 ± 7.4	36.9 ± 7.4	12.8 ± 5.1	20.7 ± 4.2	23.6 ± 9.4	—	23.1 ± 9.2
4	219.8 ± 43.9	22.9 ± 4.6	52.6 ± 10.5	52.9 ± 10.6	28.4 ± 11.4	29.1 ± 5.8	28.7 ± 11.5	37.5 ± 15.0	35.2 ± 14.1
5	220.5 ± 44.1	22.5 ± 4.5	51.3 ± 10.3	53.1 ± 10.6	27.4 ± 11.0	27.6 ± 5.5	35.9 ± 14.4	35.9 ± 14.4	25.4 ± 10.2
6	118.3 ± 23.7	18.2 ± 3.6	—	37.9 ± 7.6	17.6 ± 7.0	22.4 ± 4.5	24.8 ± 9.9	26.8 ± 10.7	26.5 ± 10.6
7	132.8 ± 26.5	17.7 ± 3.6	39.7 ± 8.0	38.6 ± 7.7	18.4 ± 7.4	22.6 ± 4.5	23.7 ± 9.5	27.9 ± 11.2	24.6 ± 9.8
8	91.0 ± 18.2	15.6 ± 3.1	34.2 ± 6.9	34.9 ± 7.0	13.8 ± 5.5	19.5 ± 3.9	27.3 ± 10.9	19.2 ± 7.7	18.9 ± 7.6
9	77.4 ± 15.5	14.3 ± 2.9	—	33.4 ± 6.7	8.1 ± 3.2	18.1 ± 3.6	16.8 ± 6.7	17.0 ± 6.8	17.3 ± 6.9

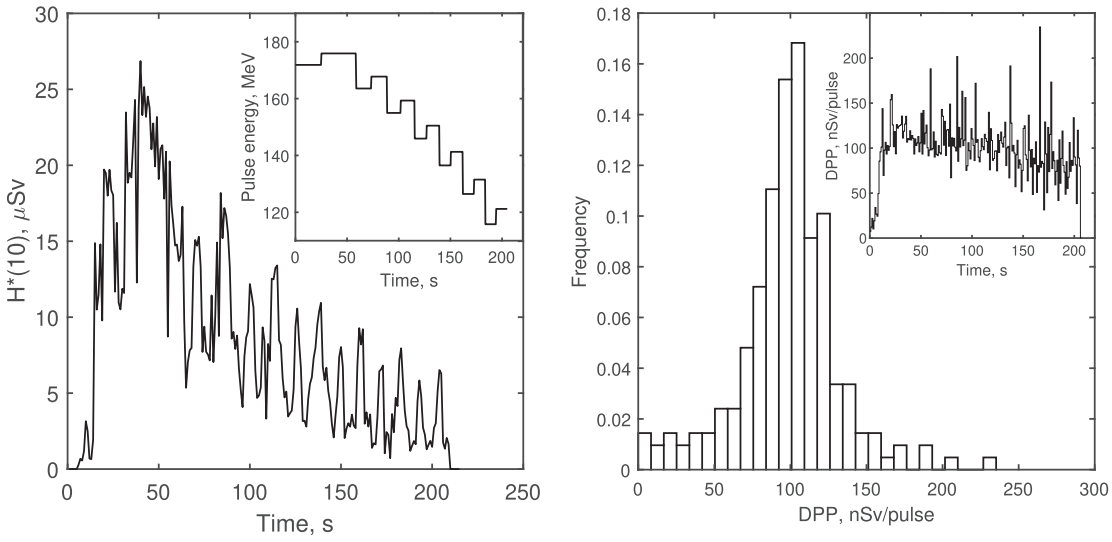

Figure 2. Left graph, main plot: H*(10) integrated over 1 s by the LUPIN at position 4 (186 cm–135°). Insert: proton energy as a function of the delivery time. Right graph, main plot: relative frequency histogram of the DPP at the same position. Insert: DPP distribution as a function of the delivery time.

20% for the extended-range rem-counters, and 40% for the conventional ones, whose response function sharply drops for neutron energies above 15–20 MeV, in accordance with previous literature studies (Silari *et al* 2009, Dinar *et al* 2018).

The main plot of the left graph of figure 2 shows H*(10) measured by the LUPIN at position 4 (186 cm–135°) as a function of time, with 1 s time resolution. This trend is representative for all positions, while the absolute values slightly vary. Fourteen peaks are clearly visible, which can be related to the fourteen energy layers of the irradiation plan (insert in the plot). The pulse delivery time was retrieved from the machine log files[12] and compared to H*(10) recorded by the LUPIN as a function of time. By dividing the recorded H*(10) by the number of pulses delivered per each second from the log files, it could be roughly estimated that the DPP reached values as high as 200 nSv/pulse. As an example, the right graph of figure 2 shows the frequency distribution of the DPP for the same position 4. This value is in the linearity range of the LUPIN, but definitely out of the linearity range of the other rem-counters, as discussed in the following subsection. The unusual trend of the dose rate with peaks and valleys can be explained considering the particular beam delivery technique, i.e. proton pulse delivery frequency ranging from 750 Hz down to roughly 2 Hz, and charge per pulse ranging from 8 pC to about 3 pC. The highest and broadest peak in the main graph of the left plot of figure 2 in the 25–75 s range is related to the highest proton energy (175.90 MeV, see the subplot in the left graph of figure 2) and to the largest delivered dose, i.e. about 30% of the total therapeutic dose at the isocentre. Its decreasing trend can be imputed to the combination of a general decrease in the pulse delivery frequency between 25 s and 75 s, and to a variable charge per pulse, which are automatically set by the machine for each specific treatment plan.

3.2. Data analysis

The left graph of figure 3 plots the data listed in table 2. Considering the experimental uncertainties, all rem-counters underestimate the dose measured by the LUPIN significantly. The variation of H*(10) as a function of measurement positions is discussed in section 3.3. The right graph of figure 3 shows the results normalised to the LUPIN output (U_{exp}) as a function of the dose measured by the LUPIN (bottom x axis) and of the average DPP (upper x axis). Since the irradiation conditions were the same for each measurement, i.e. same treatment plan, number of pulses, and delivered therapeutic dose, the total dose is proportional to the average DPP, and both depend on position. Focusing on one rem-counter at a time, a clear trend can be observed: the higher the DPP, the larger the underestimation. This trend is more evident if one neglects the systematic sources of uncertainty (i.e. from calibration and response function), leaving only the experimental one (a few percent)[13].

[12] Together with other information (pulse energy, charge, spatial coordinate, etc), the log files collect the delivery time of each single pulse, with ms time resolution.

[13] Uncertainties related to the calibration procedure and to the response function are taken into account while considering the rem-counter readout with respect to the true physical/operational quantity. In this sense they play a role when comparing two or more rem-counters. When comparing different and independent values of a given quantity collected by the same rem-counter, the only uncertainty which should be introduced is the experimental one.

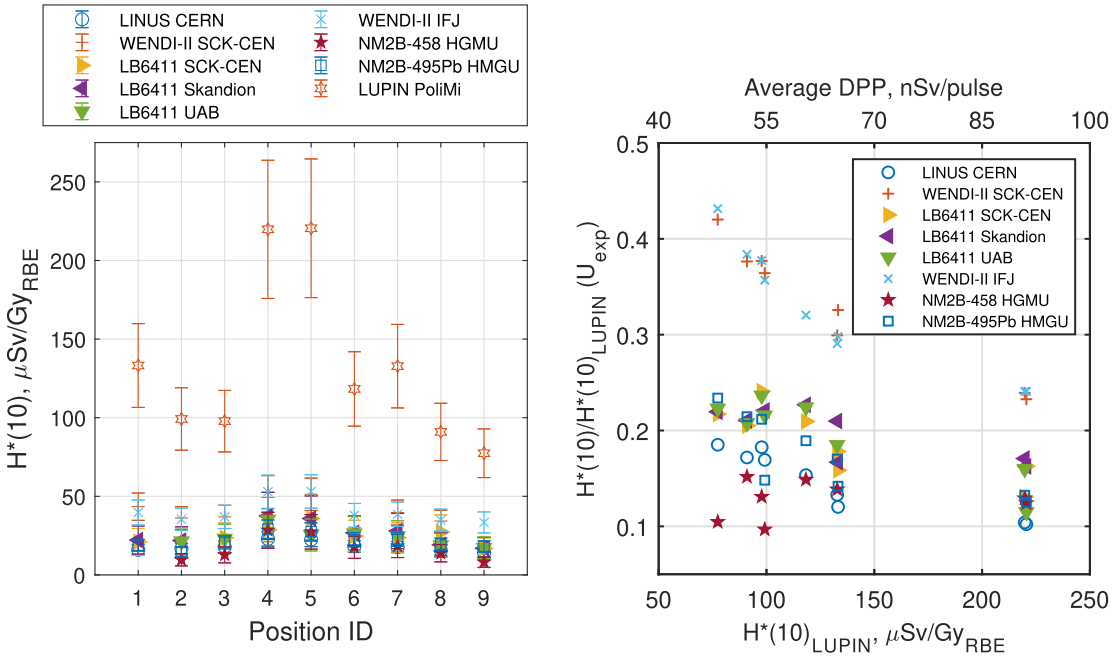

Figure 3. Results of the intercomparison. The left graph shows the neutron H*(10), normalized to unit therapeutic dose at the isocentre, measured by the nine rem-counters as a function of the position around the isocentre (figure 1). The graph on the right shows the results normalised to the dose measured by the LUPIN (the uncertainties are not shown for clarity). Conventional rem-counters are shown as full symbols; extended range rem-counters are shown as open symbols.

From the right plot of figure 3, the dependence of the WENDI-IIs' response on the DPP appears to be almost linearly decreasing. Conversely, the other rem-counters show a flatter response versus the DPP. This is in line with the data and the model presented in Caresana *et al* (2014). For rem-counters which possess a much lower D_{half} with respect to the reference DPP, the H*(10) underestimation is larger, but the response variations versus DPP are less pronounced, i.e. they reach a saturation value. These trends can be explained by DPP values estimated to be as high as 200 nSv/pulse, and D_{half} values in the range 5–30 nSv/pulse (LINUS, LB6411) and 40 nSv/pulse (WENDI-II).

In the case of the LUPIN, D_{half} is larger than 1800 nSv/pulse and therefore the LUPIN can be used as the reference instrument in the present experiment, i.e. the correction from D_{meas} to D_{ref} is only about 1.1 at 200 nSv/pulse DPP. On the opposite, for a rem-counter with D_{half} equal to 40 nSv/pulse and DPP equal to 200 nSv/pulse, equation (1) estimates a correction factor of about 6 to go from D_{ref} to D_{meas}, i.e. this rem-counter measures about 15% of the reference DPP.

For conventional rem-counters (full symbols in figure 3), the underestimation can be imputed to two effects:

1. Dead time losses due to the pulsed time profile of the stray neutron field.
2. Intrinsic low sensitivity to high energy neutrons.

For extended range rem-counters, the underestimation is due to pulsed field only, even if small differences can remain because of the different response function of different rem-counter models.

Thus, the question to address is: can the model proposed by Caresana *et al* justify the experimental underestimation measured in this work? To answer this question, $U_{model,k,j}$ was calculated for each rem-counter and for each position following the model of section 2.4. $U_{model,k,j}$ is then compared with the measured underestimation U_{exp} and presented as scatter plots in figure 4. If points are on the bisector, it means that the experimental underestimation agrees with the underestimation foreseen by the model. If points are above/below the bisector, the experimental underestimation is larger/smaller than the one foreseen by the model.

It can be noted that the conventional rem-counters underestimate more severely than the extended range rem-counters, and more severely than the model prediction. As mentioned above, this is due to the combination of dead time losses and intrinsic low sensitivity to high energy neutrons. This effect is particularly evident while comparing NM2B-498 (conventional) and NM2B-495Pb (extended range), which share the same electronics and are thus similarly affected by dead time losses. Extended range rem-counters are in better agreement and small differences can be ascribed to small differences in their response functions. Only the LINUS appears to be quite well described by the model because LINUS and LUPIN have a quite similar response function.

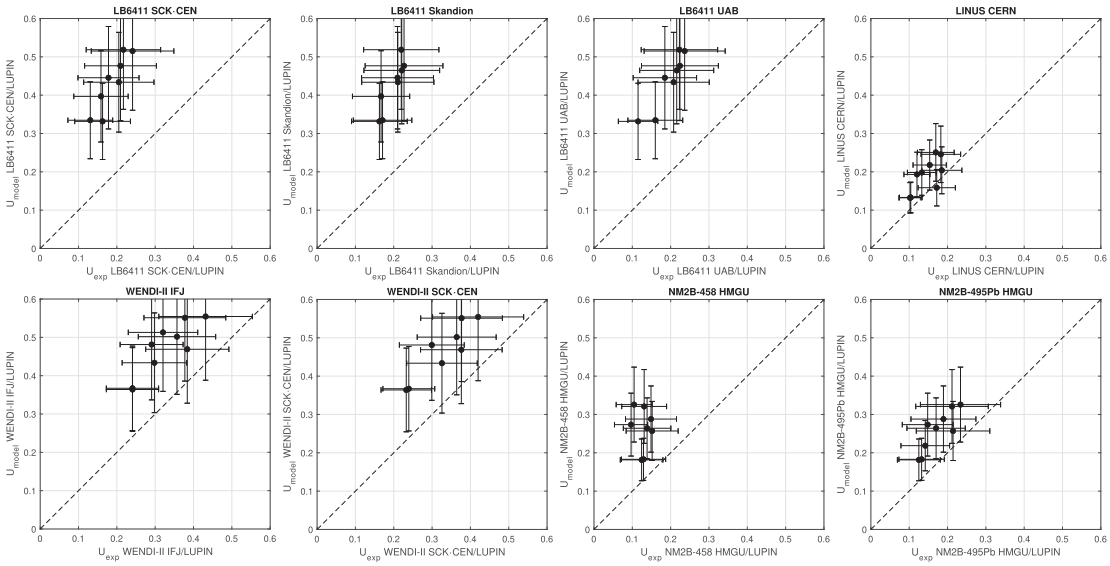

Figure 4. Scatter plots of the rem-counter measurements. The *x* coordinate is the experimental result, the *y* coordinate the calculated value. Uncertainties are shown as ± 1 standard deviation around the measured value ($k = 1$); they account for calibration, position and angular/energy response functions of the rem-counters. They can be assumed to be 20% for the extended-range rem-counters, and 40% for the conventional ones (Mayer *et al* 2005, Silari *et al* 2009, Dinar *et al* 2018), with a further increase considering the uncertainty propagation, since U_{exp} and U_{model} are fractional numbers.

However, the model accounts only for the dead time losses due to the pulsed field and not for the different response functions. In order to better compare with the model, the two contributions to the underestimation must be separated. This is done by considering the response functions of the various rem-counters. The response functions approximate the ICRP $h^*(10)$ coefficients in a broad range of neutron energies, but discrepancies up to 40% between the reference and the measured $H^*(10)$ are sometimes observed (see for example Dinar *et al* (2018)). In the experiment described in Caresana *et al* (2014), neutrons were produced by 60 MeV monoenergetic protons impinging on a thick tungsten target, with the detectors[14] placed downstream of it, centred at beam height. Roughly one half of the reference $H^*(10)$ was due to evaporation neutrons, and the other half to neutrons with energies in the range 20–60 MeV. Moreover, the reference $H^*(10)$ value was estimated by averaging the read-out of all neutron detectors.

In the present experiment, the reference $H^*(10)$ was estimated by the LUPIN with a nominal 20% uncertainty. Moreover, the neutron spectra obtained during the spectrometry measurements (EURADOS WG9-WG11 2022) performed during the same experimental campaign at Maastro[15] were quite different from the spectra described in Caresana *et al* (2014), with the predominant contribution from evaporation neutrons. Consequently, equation (3) should be modified by introducing correction factors $C_{f,k,j}$ calculated for each position k and for each rem-counter j as the ratio between the reference dose and the dose measured by the jth rem-counter compensated by folding its response function[16] with the neutron spectrum from EURADOS WG9-WG11 (2022) in the kth position. The reference dose is obtained by folding the neutron spectrum at a given position k with the $h^*(10)$ coefficients (ICRP-74 1996, ICRU-57 2016).

It is worth noting that the experimental conditions of the spectrometry experiment were partially different from the rem-counter intercomparison, i.e. irradiation of a 5 cm $\times$ 5 cm $\times$ 5 cm target volume in an anthropomorphic phantom. However, from a previous experiment, the spectral energy distribution of secondary neutrons was observed to remain similar when varying the target volume and/or the phantom (Mares *et al* 2016). Therefore, the spectra from the spectrometry experiment can be used as a reference for the calculations with reasonable confidence. Considering the variation of up to about 15% of the $h^*(10)$ coefficients in the energy range from 125 MeV to 160 MeV, the average proton energies in the spectrometry and rem-counter experiments respectively, and considering the uncertainties related to calibration, position and angular response of the instruments, a 20% uncertainty was conservatively assumed for the results of the calculations. In

[14] In that study, rem-counters were tested together with other types of neutron monitors.

[15] As mentioned in section 1, ambient dosimetry measurements at Maastro were performed by rem-counters (discussed in this paper) and Bonner spheres, complemented by Monte Carlo calculations (discussed in detail in a forthcoming paper (EURADOS WG9-WG11 2022)).

[16] The LUPIN, LINUS and the two NM2Bs were characterised during previous measurements and their response functions were available to the authors. For the LB6411 data were taken from Burgkhardt *et al* (1997), for the WENDI-II from Jägerhofer *et al* (2011).

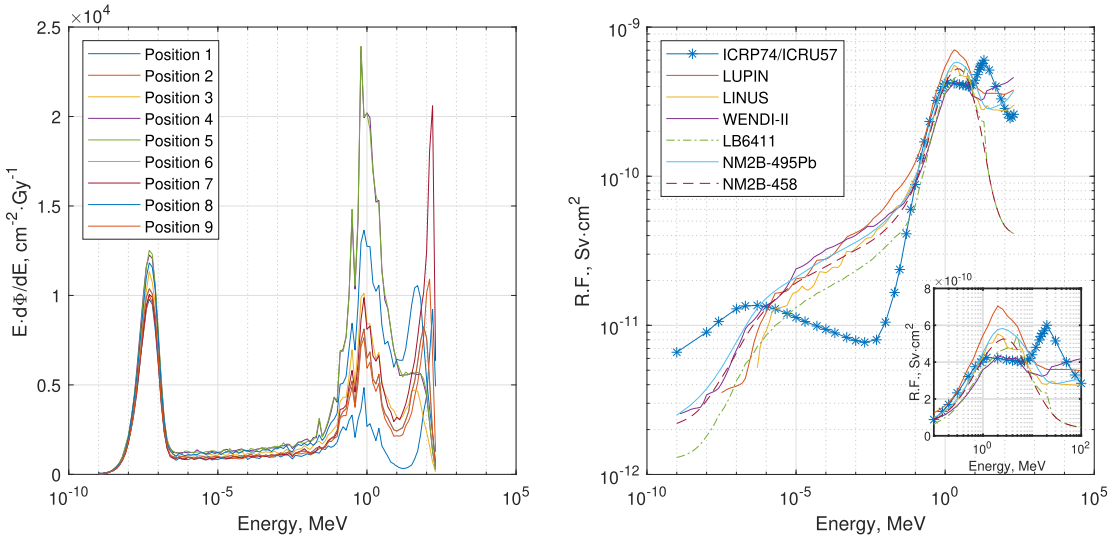

Figure 5. Left figure: neutron spectra obtained during the spectrometry experiment (EURADOS WG9-WG11 2022). The spectra were folded with the response function of each rem-counter and the ICRP $h^*(10)$ coefficients (right figure) to obtain the correction factors $C_{f,k,j}$ (see text). The insert in the right figure is the detail of the response functions in the evaporation region, which corresponds to the largest contribution to the neutron dose in this experiment.

Table 3. Correction factors $C_{f,k,j}$ calculated for the whole set of rem-counters. k runs over the positions and j over the rem-counters. The last two columns, listing the correction factors for the conventional rem-counters, show the highest values, i.e. the largest discrepancies between the $h^*(10)$ coefficients and the rem-counters' response function.

Position	LUPIN	LINUS	WENDI-II	NM2B-495Pb	NM2B-458	LB6411
1	0.75	0.95	0.87	0.87	1.40	1.58
2	0.82	1.04	0.99	0.96	1.46	1.60
3	0.83	1.04	1.11	0.97	1.23	1.35
4	0.80	1.01	1.12	0.94	1.15	1.26
5	0.82	1.05	0.95	0.95	1.58	1.50
6	0.84	1.06	1.04	0.99	1.41	1.55
7	0.80	1.01	1.12	0.94	1.15	1.26
8	0.86	1.08	1.11	1.01	1.35	1.46
9	0.84	1.06	1.04	0.99	1.41	1.55

the case of the LB6411s, the response function was extrapolated for energies above 40 MeV, which is the highest energy available in Burgkhardt *et al* (1997), and thus an additional 10% uncertainty was assumed[17].

Figure 5 left shows the lethargy plot of the neutron spectra obtained from the spectrometry experiment at each position (EURADOS WG9-WG11 2022). Figure 5 right shows the response functions of the rem-counters used in the present study compared to the ICRP $h^*(10)$ coefficients (ICRP-74 1996, ICRU-57 2016). It can be observed that from 0.1 MeV up to 10–15 MeV all rem-counters satisfactorily approximate the $h^*(10)$ coefficients. For higher energies, the response function of conventional rem-counters (LB6411 and NM2B-458, dash-dotted and dashed lines in the figure, respectively) decreases significantly.

The full set of the calculated correction factors is listed in table 3. The correction factors reflect the discrepancy between the $h^*(10)$ coefficients (reference $H^*(10)$) and the rem-counters' response function (measured $H^*(10)$) in the present experimental conditions. As expected, for extended-range rem-counters the discrepancy between reference and measured $H^*(10)$ is of the order of 20%, while for conventional rem-counters it can be as high as 40%–50%.

For position k, $C_{f,k,ref}$ is the correction factor of the LUPIN, while $C_{f,k,j}$ is the correction factor of the rem-counter j. $D_{ref,i,k}$ is evaluated from equation (2) by correcting $D_{LUPIN,i,k}$ for $C_{f,k,ref}$. $D_{ref,i,k}$ is then used for calculating $D_{meas,i,k,j}$ from equation (1). Eventually, equation (3) becomes:

[17] The introduced uncertainties might appear quite overestimated. However, the goal of these calculations was to compare our experimental trends with literature data obtained in different experimental conditions (Caresana *et al* 2014), and not to propose mathematical models to accurately predict $H^*(10)$ with rem-counters affected by large underestimations in pulsed fields.

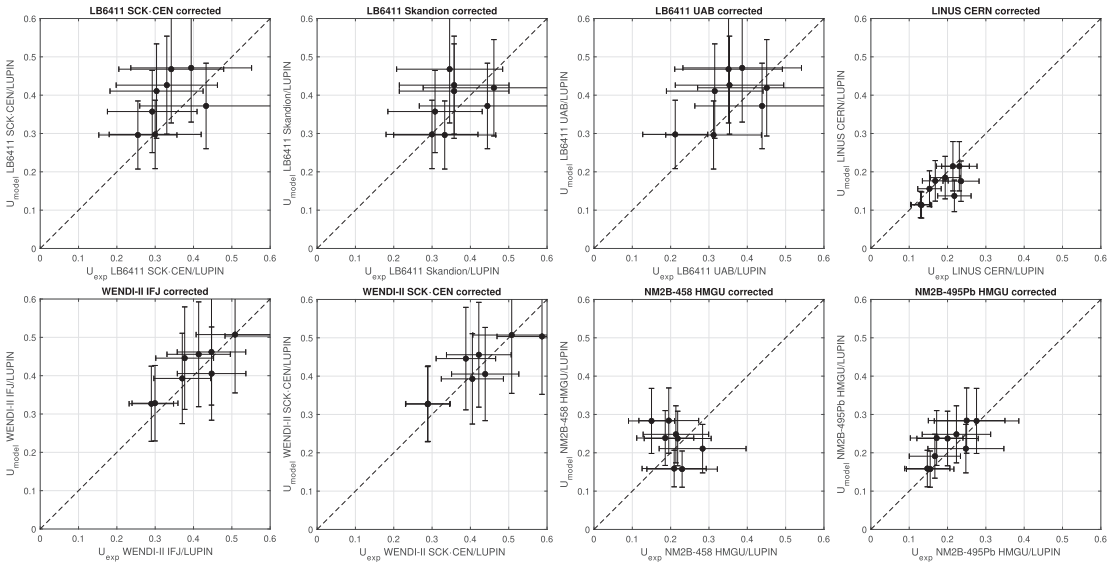

Figure 6. Scatter plots of the rem-counter measurements after applying the correction factors of the response functions. The *x* coordinate is the experimental result, the *y* coordinate the calculated value. Uncertainties are shown as ± 1 standard deviation around the measured value ($k = 1$); they conservatively account for the 15% difference between the $h^*(10)$ coefficients at the average proton energy of the present experiment versus the spectrometry one (EURADOS WG9-WG11 2022), and for the position and angular dependence of the response functions of rem-counters. The uncertainty can be assumed to be 20% for all rem-counters except for the LB6411s, whose response function was extrapolated for energies above 40 MeV (i.e. the LB6411 uncertainty was enhanced to 30%). A further increase of the final uncertainty was due to uncertainty propagation, since U_{exp} and U_{model} are fractional numbers.

$$U_{model,k,j} = \frac{\sum_i^N D_{model,i,k,j} \cdot C_{f,k,j}}{\sum_i^N D_{LUPIN,i,k} \cdot C_{f,k,ref}}. \tag{4}$$

This new formulation of $U_{model,k,j}$ includes the effect of the response function on the rem-counters and permits to highlight the underestimations generated only by the dead time losses in the pulsed field. The same representation of figure 4 is proposed in figure 6, with the new formulation of $U_{model,k,j}$ of equation (4) on the *y* axis. The *x* axis has been modified and plots the quantity from equation (5)

$$U_{exp,k,j} = \frac{D_{meas,k,j} \cdot C_{f,k,j}}{D_{LUPIN,k} \cdot C_{f,k,ref}} \tag{5}$$

that is, also the experimental underestimation has been corrected by the response function of the rem-counters.

3.3. Discussion

After the introduction of the correction factors, almost all results are correctly aligned along the bisector (figure 6), meaning that the model correctly foresees the measured underestimation. Therefore, the DPP at the Maastro facility was correctly estimated based on the data collected by the LUPIN within 20% confidence. Under controlled irradiation conditions, D_{half} can be used to evaluate the capability of an instrument to withstand a pulsed neutron field with a certain average DPP in a certain neutron energy spectrum. However, the DPP is typically an unknown quantity, in particular when the neutron field is a stray/secondary field, as in the case of proton therapy facilities; neutron spectrometry requires specific experiments using Bonner spheres, usually combined with Monte Carlo calculations. Therefore, even if the above calculations could in principle be performed for correcting the rem-counter measurements, at most workplaces the required information for the correct modelling is missing. Consequently, the type of rem-counter should be carefully chosen, because in most cases there is no possibility of correcting the measurement *a posteriori* to retrieve the reference (conventionally true) $H^*(10)$. Furthermore, correcting a rem-counter measurement affected by extremely high underestimations (e.g. up to 90%, see figure 3) unavoidably adds large uncertainties. For these reasons, extended-range rem-counters specifically designed to withstand pulsed neutron fields should be preferred for measurements at the Mevion S250i and similar accelerators. As a second outcome, the calculated correction factors for the LUPIN, in the range 0.75–0.85, reflect that in this type of facilities this rem-counter can measure the reference $H^*(10)$ with a maximum overestimation of the order of 20%, adequate for radiation protection purposes.

The highest doses were measured at positions 4 and 5, i.e. near the beam delivery system (figure 1). In contrast, at position 1 the measured dose was only about 60% of that at positions 4 and 5. This suggests that the

largest contribution to H*(10) was due to external neutrons from the beam delivery system. The quite small differences between the doses measured at positions 6, 7 and 8 when compared to the symmetric positions 3, 2 and 9 can be explained by the asymmetry of the water tank phantom, as shown in figure 1. The differences are within 20%, so that the phantom asymmetry effect (i.e. about 7.5 cm of water in position 6 versus 37.5 cm of water in position 3) lies within the rem-counter uncertainty (figure 3).

4. Comparisons with other proton therapy facilities

In this section, the values of H*(10) measured at Maastro are compared with literature data available for other proton therapy facilities. Section 4.1 is dedicated to a comparison between the Maastro H*(10) and measurements at similar Mevion facilities. Section 4.2 compares our results with other EURADOS experiments, which were performed with different accelerator types, but in which the experimental setup and beam parameters were almost equivalent to the ones of the current measurements.

4.1. Comparison with other Mevion facilities

Only a few neutron experiments are reported in the literature with the rather new Mevion systems. H*(10) values of about 150–200 μSv/Gy$_{RBE}$ at 2 m distance measured in the present study partially agree with values reported in studies performed by other groups at similar Mevion S250 facilities (Chen *et al* 2013, Howell *et al* 2016, Prusator *et al* 2018). The Mevion S250 has the same gantry-mounted synchrocyclotron as the Mevion S250i, but it is equipped with a purely passive beam delivery system.

Prusator *et al* (2018) demonstrated via Monte Carlo calculations that H*(10) increases from 0° to 135° with respect to the beam direction, in line with the LUPIN results of the present study. This supports the assumption that most of H*(10) is due to external neutrons. Chen *et al* (2013) and Howell *et al* (2016) further confirmed this hypothesis with their spectrometry measurements, which showed that most of H*(10) is due to evaporation neutrons in almost all positions around the isocentre.

Chen *et al* measured the neutron H*(10) at one metre from the isocentre. They observed a variation of H*(10) from a few hundred μSv/Gy up to a few mSv/Gy. The reason of such large variation can be imputed to the purely passive beam delivery modality.

In the study by Prusator *et al*, the comparison between Monte Carlo simulations and measurements performed with a WENDI-II showed the same trends in all locations around the isocentre. However, the measured values were about 10 times lower than the simulated ones for all positions. They measured about 200–300 μSv/Gy at one meter, while Monte Carlo calculations estimated neutron H*(10) of the order of 2–3 mSv/Gy. The authors suspected that the simulated neutron source terms were too simplistic. However, considering that the time structure of the Mevion S250 and S250i proton beams is the same[18], it cannot be excluded that the instrument employed could have underestimated the true H*(10) because of the pulsed structure of the neutron field if the pulse charge was not substantially lowered with respect to the standard clinical settings.

Chen *et al* (2013) performed similar measurements. It is worth noting that 'Configuration C' in Chen *et al* (2013) is analogous to 'Configuration large' in Prusator *et al* (2018), both with a treatment configuration characterized by 20 cm modulation range, 25 cm isocentre depth, and use of a large applicator. In this condition, at 1 m from the isocentre and at 90° with respect to the beam axis, Chen *et al* calculated by Monte Carlo simulations a neutron H*(10) equal to 3 mSv/Gy. On the other hand, Prusator *et al* measured 350 μSv/Gy. Since Prusator *et al* stated that their Monte Carlo estimations of H*(10) were about ten times larger than the experimental results, they should have calculated H*(10) equal to about 3.5 mSv/Gy. Therefore, the good agreement between the calculations made by Chen *et al* and Prusator *et al* might suggest that the WENDI-II used in the experiment of Prusator *et al* may have been affected by pile up due to the pulsed structure of the neutron field.

However, the Monte Carlo calculations of Chen *et al* were in turn validated by measurements made with a WENDI-II, but in the article the authors explicitly state that the dose rate was decreased to avoid pile up. If the pulse charge was decreased to lower the dose rate, the neutron DPP decreased too, and consequently the WENDI-II should have correctly measured H*(10). Nevertheless, we demonstrated that in the case of pulsed fields, where the DPP is usually complex to be correctly derived, the dose rate is a secondary parameter, and devices specifically designed to withstand pulsed fields should always be preferred.

[18] Both systems provide 227 MeV pulsed proton beams at 10 μs pulse width (private communication from Mevion).

4.2. Comparison with other EURADOS experiments

Since 2015 EURADOS has been promoting similar intercomparison exercises at some of the newest proton therapy facilities across Europe. In some cases, similar experimental conditions allow for a detailed comparisons of neutron production between different accelerator types. For example, the experiment described in Farah *et al* (2015) was performed employing an IBA (Ion Beam Applications SA, Louvain-La-Neuve, Belgium) cyclotron at the Trento Proton Therapy Centre in Italy, with a similar treatment plan (10 cm $\times$ 10 cm $\times$ 10 cm cube centred at 10 cm depth in water, maximum beam energy about 172 MeV) and employing the same water tank phantom as in the present work. This accelerator delivers the proton beam with the required energy using an energy selection system located between the cyclotron and the treatment room. The neutron $H^*(10)$ at a position approximately equivalent to position 1 in the present experiment was equal to 50 μSv/Gy, which then dropped to 8 μSv/Gy, 3 μSv/Gy and 5 μSv/Gy at positions approximately equivalent to positions 2, 3 and 4, respectively. Therefore, in their experiment the stray neutron dose was dominated by forward-peaked high-energy internal neutrons. It is interesting to note that the total neutron $H^*(10)$ was about one half of that measured in the present study at position 1, falling to 8%–2% for positions 2, 3 and 4, where the contribution of high-energy neutrons becomes less significant. Similar results were obtained at the IBA cyclotron at the Cyclotron Centre Bronowice, Poland, with $H^*(10)$ equal to 72 μSv/Gy, 14 μSv/Gy, 8 μSv/Gy and 21 μSv/Gy at positions approximately equivalent to positions 1, 3, 4, and 6, respectively (200 MeV protons with beam size 20 cm $\times$ 20 cm) (Mojżeszek *et al* 2017). Another experiment involving an active energy selection system (VARIAN Medical Systems Particle Therapy GmbH) was performed at the Rinecker Proton Therapy Centre in Munich, Germany (Trinkl *et al* 2017). A 30 cm $\times$ 30 cm $\times$ 15 cm PMMA slab phantom was used to simulate the patient. The neutron $H^*(10)$ was measured with a Bonner sphere spectrometer. For 200 MeV protons, the highest $H^*(10)$ of 24 μSv/Gy was measured at a position approximately equivalent to position 1 in the present experiment, and the lowest of 4.10 μSv/Gy at a position approximately equivalent to position 4. For 140 MeV protons, $H^*(10)$ was equal to 5.9 μSv/Gy and 1.5 μSv/Gy at positions equivalent to 1 and 4 respectively.

In the experiment described in Mojżeszek *et al* (2017), a WENDI-II correctly measured $H^*(10)$ within 20% uncertainty in a steady-state field[19]. In the experiment described in Farah *et al* (2015), different commercial rem-counters were used. Extended range rem-counters (WENDI-II, NM2B-495Pb) correctly estimated $H^*(10)$ with discrepancies from the reference $H^*(10)$ below 20%. For conventional rem-counters (LB6411, NM2B-458), underestimations of the reference $H^*(10)$ from 40% to 50% were observed, in line with the correction factors listed in table 3. This underlines once more the importance of having the best available *a priori* knowledge of the neutron field, both in terms of energy and time structure. Extended range rem-counters which were observed to correctly assess $H^*(10)$ in a steady-state field, underestimated the reference $H^*(10)$ up to 75% (WENDI-II) and 90% (LINUS) at the Maastro facility.

The results obtained in the present study for positions 2 and 4 can also be compared with those obtained in an experiment performed at the Centre de Proton Thérapie d'Orsay, France, where an IBA cyclotron with a passive-scattering dose delivery system was used with similar beam settings (10 cm $\times$ 10 cm $\times$ 10 cm cube centred at 10 cm depth in water, maximum beam energy about 172 MeV) and employing the same water tank phantom as in the present work (Farah *et al* 2015). A value of $H^*(10)$ of 167 μSv/Gy was measured at a location equivalent to position 2, quite in line with the result of the present experiment (99.2 $\pm$ 19.8 μSv/Gy for the LUPIN), while at a location equivalent to position 4, $H^*(10)$ was equal to 29.6 μSv/Gy (while it was 219.8 $\pm$ 43.9 μSv/Gy for the LUPIN in the present experiment). This obvious discrepancy for position 4 might be imputed to the particular configuration of the Mevion S250i synchrocyclotron, which is mounted inside the treatment room (Vilches-Freixas *et al* 2020), so that the stray neutrons from the accelerator are not shielded as in the case of a separate vault housing the accelerator (as at the Centre de Proton Thérapie d'Orsay).

5. Conclusions

In proton therapy facilities the dose due to secondary neutrons should be accurately monitored, to assess the dose to both the patient and the medical staff. Rem-counters are usually employed for benchmarking Monte Carlo calculations, performing shielding verifications and routine neutron dose monitoring. They are robust, portable, with a negligible gamma-ray sensitivity, and their response function follows with reasonable approximation the ICRP $h^*(10)$ coefficients. However, *a priori* knowledge of the neutron field is required for the proper choice of the instrument, in particular with respect to its response to high-energy neutrons and its behaviour in pulsed fields.

[19] Cyclotrons accelerate proton bunches at frequencies of the order of hundred MHz. Hence, considering a typical dead time of the order of 5–15 μs, the stray neutron field is perceived by a rem-counter as steady-state, i.e. non-pulsed.

This work presents the results of an intercomparison of various commercial and non-commercial rem-counters (LUPIN, LINUS, WENDI-II, LB6411, NM2B-458, NM2B-495Pb) in a proton therapy facility simulating a patient treatment protocol with clinical beam settings. The accelerator employed, a synchrocyclotron of the type Mevion S250i, is a compact system directly mounted on the gantry. The beam is delivered with a pulsed structure, and the energy modulation is obtained by an energy degrader.

Among the tested rem-counters, only the LUPIN measured the true $H^*(10)$ within a 20% uncertainty. All other rem-counters underestimated the neutron $H^*(10)$ by factors from 2 to 10 mostly because of dead time losses, depending on both the rem-counter model and the neutron DPP. DPP values as high as 200 nSv/pulse were measured, which make most commercial rem-counters inadequate for measuring neutron doses (for the majority of commercial rem-counters the D_{half} value lies between 5 and 40 nSv/pulse). Conventional rem-counters, i.e. those without high-Z converters, have the additional limitation of very low sensitivity above 15 MeV, resulting in significant underestimation of the neutron dose (even more than 50%).

The model from Caresana *et al* (2014) was used to predict the underestimation of rem-counters, assuming the LUPIN response as reference, unaffected by dead time losses. The model has proved to work well for all rem-counters. This is a strong indication that the LUPIN is the only tested instrument capable of measuring in this workplace field without the need of any correction based on machine parameters or measurement position. In principle, if the investigator is prepared to accept large uncertainties, it is possible to use rem-counters other than the LUPIN. However, the correction procedure is quite complex (section 3.2) and needs at least the machine log files, a real-time reading of $H^*(10)$, and information about the neutron spectrum to correct each radiation pulse. This complexity prevents any practical use in workplace scenarios where details of the radiation field are often unknown. As a consequence, the type of rem-counter should be carefully chosen, because in most cases there is no possibility of correcting *a posteriori* the measured $H^*(10)$ to retrieve the actual $H^*(10)$. In general, rem-counters specifically designed for pulsed neutron fields are the only option.

The $H^*(10)$ measured by the LUPIN was found in partial agreement with results of similar experiments performed at other Mevion facilities employing passive energy modulation. Comparisons of the neutron doses obtained in the present study with those reported for facilities employing active energy selection systems confirmed that the neutron $H^*(10)$ is more than a factor of 10 higher at facilities using passive energy degradation for dose delivery. Comparisons with an experiment with passive energy modulation confirmed that the $H^*(10)$ was similar downstream of the patient, i.e. far from the accelerator. However, for positions closer to the accelerator, the $H^*(10)$ obtained in the present study was larger by a factor of 10 as compared to $H^*(10)$ at facilities in which the accelerator is housed in a separately shielded vault. This is due to the particular structure of the Mevion S250i Hyperscan synchrocyclotron, which is mounted directly on the gantry, i.e. inside the treatment room.

ORCID iDs

Gabriele Zorloni https://orcid.org/0000-0001-5983-9837
Marco Caresana https://orcid.org/0000-0002-6860-7859
Renata Kopec https://orcid.org/0000-0002-0919-9859
Pawel Olko https://orcid.org/0000-0001-5554-8178
Miguel Angel Caballero-Pacheco https://orcid.org/0000-0002-2433-1125
Liliana Stolarczyk https://orcid.org/0000-0002-6333-3350
Sebastian Trinkl https://orcid.org/0000-0001-5352-5490

References

Aza E, Caresana M, Cassell C, Charitonidis N, Harrouch E, Manessi G P, Pangallo M, Perrin D, Samara E and Silari M 2014 Instrument intercomparison in the pulsed neutron fields at the CERN HiRadMat facility *Radiat. Meas.* **61** 25–32

Birattari C, Esposito A, Ferrari A, Pelliccioni M, Rancati T and Silari M 1998 The extended range neutron rem counter 'LINUS': overview and latest developments *Radiat. Prot. Dosim.* **76** 135–48

Birattari C, Esposito A, Ferrari A, Pelliccioni M and Silari M 1992 A neutron survey meter with sensitivity extended up to 400 MeV *Radiat. Prot. Dosim.* **44** 193–7

Birattari C, Esposito A, Ferrari A, Pelliccioni M and Silari M 1993 Calibration of the neutron rem counter LINUS in the energy range from thermal to 19 MeV *Nucl. Instrum. Methods Phys. Res. A* **324** 232–8

Birattari C, Ferrari A, Nuccetelli C, Pelliccioni M and Silari M 1990 An extended range neutron rem counter *Nucl. Instrum. Methods Phys. Res. A* **297** 250–7

Burgkhardt B, Frieg G, Klett A, Plewnia A and Siebert B R L 1997 The neutron fluence and $H^*(10)$ response of the new LB 6144 REM counter *Radiat. Prot. Dosim.* **70** 361–4

Caresana M *et al* 2014 Intercomparison of radiation protection instrumentation in a pulsed neutron field *Nucl. Instrum. Methods Phys. Res. A* **737** 203–13

Caresana M, Ferrarini M, Manessi G P, Silari M and Varoli V 2013a LUPIN, a new instrument for pulsed neutron fields *Nucl. Instrum. Methods Phys. Res. A* **712** 15–26
Caresana M, Ferrarini M, Manessi G P, Silari M and Varoli V 2013b A neutron detector for pulsed mixed fields: preliminary measurements *Progress in Nuclear Science and Technology* **4** 725–8
Caresana M, Helmecke M, Kubancak J, Manessi G P, Ott K, Scherpelz R and Silari M 2014b Instrument intercomparison in the high-energy mixed field at the CERN-EU reference field (CERF) facility *Radiat. Prot. Dosim.* **161** 67–72
Carnicer A, Letellier V, Rucka G, Angellier G, Sauerwein W and Herault J 2012 Study of the secondary neutral radiation in proton therapy: toward an indirect *in vivo* dosimetry *Med. Phys.* **39** 7303–16
Chen K, Bloch C, Hill P and Klein E 2013 Evaluation of neutron dose equivalent from the Mevion S250 proton accelerator: Measurements and calculations *Phys. Med. Biol.* **58** 8709–23
Dinar N, Pozzi F, Silari M, Puzo P, Chiriotti S, De Saint-Hubert M, Vanhavere F, Van Hoey O, Orchard G M and Waker A J 2018 Instrument intercomparison in the high-energy field at the CERN-EU reference field (CERF) facility and comparison with the 2017 FLUKA simulations *Radiat. Meas.* **117** 24–34
EURADOS WG9-WG11 2022 (in preparation)
Farah J *et al* 2015 Measurement of stray radiation within a scanning proton therapy facility: EURADOS WG9 intercomparison exercise of active dosimetry systems *Med. Phys.* **42** 2572–84
Ferrarini M, Varoli V, Favalli A, Caresana M and Pedersen B 2010 A wide dynamic range BF3 neutron monitor with front-end electronics based on a logarithmic amplifier *Nucl. Instrum. Methods Phys. Res. A* **613** 272–6
Gottschalk B 2006 Neutron dose in scattered and scanned proton beams: in regard to Eric J. Hall (Int J Radiat Oncol Biol Phys 2006;65:1–7) *Int. J. Radiat. Oncol. *Biol.* Phys.* **66** 1594
Hälg R and Schneider U 2020 Neutron dose and its measurement in proton therapy—current state of knowledge *Br. J. Radiol.* **93** 20190412
Hall E J 2006 Intensity-modulated radiation therapy, protons, and the risk of second cancers *Int. J. Radiat. Oncol. *Biol.* Phys.* **65** 1–7
Howell R M, Burgett E A, Isaacs D, Price Hedrick S G, Reilly M P, Rankine L J, Grantham K K, Perkins S and Klein E E 2016 Measured neutron spectra and dose equivalents from a Mevion single-room, passively scattered proton system used for craniospinal irradiation *Int. J. Radiat. Oncol. *Biol.* Phys.* **95** 249–57
ICRP-74 1996 Conversion coefficients for use in radiological protection against external radiation. ICRP publication 74 *Ann. ICRP* 26 (3-4)
ICRU-57 1998 *Conversion coefficients for use in radiological protection against external radiation* ICRU Report 57 Bethesda, U.S.A
Jägerhofer L *et al* 2011 Characterization of the WENDI-II REM Counter for its Application at MedAustron *Prog. Nucl. Sci. Technol.* **2** 258–62
Jarlskog C Z and Paganetti H 2008 Risk of developing second cancer from neutron dose in proton therapy as function of field characteristics, organ, and patient age *Int. J. Radiat. Oncol. *Biol.* Phys.* **72** 228–35
Justus A L 2012 Count rate limitations for pulse-counting instrumentation in pulsed accelerator fields *Health Phys.* **102** 8–24
Knoll G F 2010 *Radiation Detection and Measurement* 4th edn (New York: Wiley)
Leake J W, Lowe T, Mason R S and White G 2010 A new method of measuring a large pulsed neutron fluence or dose exploiting the die-away of thermalized neutrons in a polyethylene moderator *Nucl. Instrum. Methods Phys. Res. A* **613** 112–8
Mares V, Romero-Expósito M, Farah J, Trinkl S, Domingo C, Dommert M, Stolarczyk L, Van Ryckeghem L, Wielunski M and Olko P 2016 A comprehensive spectrometry study of a stray neutron radiation field in scanning proton therapy *Phys. Med. Biol.* **61** 4127–40
Mares V, Sannikov A V and Schraube H 2002 Response functions of the Andersson–Braun and extended range rem counters for neutron energies from thermal to 10 GeV *Nucl. Instrum. Methods Phys. Res. A* **476** 341–6
Mares V, Trinkl S, Iwamoto Y, Masuda A, Matsumoto T, Hagiwara M, Satoh D, Yashima H, Shima T and Nakamura T 2017 Neutron spectrometry and dosimetry in 100 and 300 MeV quasi-mono-energetic neutron field at RCNP, Osaka University, Japan *EPJ Web Conf.* **153** 08020
Mayer S, Forkel-Wirth D, Fuerstner M, Menzel H G, Roesler S, Theis C and Vincke H 2005 Performance tests of survey instruments used in radiation fields around high-energy accelerators *Proc. of 2005 Particle Accelerator Conf. (Knoxville, Tennessee)*
Mojżeszek N, Farah J, Kłodowska M, Ploc O, Stolarczyk L, Waligórski M P R and Olko P 2017 Measurement of stray neutron doses inside the treatment room from a proton pencil beam scanning system *Phys. Med.* **34** 80–4
Olsher R H, Hsu H H, Beverding A, Kleck J H, Casson W H, Vasilik D G and Devine R T 2000 WENDI: an improved neutron rem meter *Health Phys.* **79** 170–81
Paganetti H, Bortfeld T and Delaney T F 2006 Neutron dose in proton radiation therapy: In regard to Eric J. Hall (Int J Radiat Oncol Biol Phys 2006;65:1–7) *Int. J. Radiat. Oncol. *Biol.* Phys.* **66** 1594–5
Paganetti H, Niemierko A, Ancukiewicz M, Gerweck L E, Goitein M, Loeffler J S and Suit H D 2002 Relative biological effectiveness (RBE) values for proton beam therapy *Int. J. Radiat. Oncol. *Biol.* Phys.* **53** 407–21
Park S H, Hyun S and Oh Kang J 2011 Basics of particle therapy: I. Physics *Radiat. Oncol. J.* **29** 135–46
Prusator M T, Ahmad S and Chen Y 2018 Shielding verification and neutron dose evaluation of the Mevion S250 proton therapy unit *J. Appl. Clin. Med. Phys.* **19** 305–10
De Saint-Hubert M *et al* 2016 Secondary neutron doses in a proton therapy centre *Radiat. Prot. Dosim.* **170** 336–41
Schneider U and Hälg R 2015 The impact of neutrons in clinical proton therapy *Front. Oncol.* **5** 235
Silari M *et al* 2009 Intercomparison of radiation protection devices in a high-energy stray neutron field: III. Instrument response *Radiat. Meas.* **44** 673–91
Trinkl S, Mares V, Englbrecht F S, Wilkens J J, Wielunski M, Parodi K, Rühm K and Hillbrand M 2017 Systematic out-of-field secondary neutron spectrometry and dosimetry in pencil beam scanning proton therapy *Med. Phys.* **44** 1912–20
Linz U (ed) 2012 *Ion Beam Therapy: Fundamentals, Technology, Clinical Applications* 1st edn (Berlin: Springer) (https://doi.org/10.1007/978-3-642-21414-1)
Vilches-Freixas G, Unipan M, Rinaldi I, Martens J, Roijen E, Almeida I P, Decabooter E and Bosmans G 2020 Beam commissioning of the first compact proton therapy system with spot scanning and dynamic field collimation *Br. J. Radiol.* **1107** 20190598